Journal of Electronic Research and Application, 2026, Volume 10, Issue 1
http://ojs.bbwpublisher.com/index.php/JERA
ISSN Online: 2208-3510
ISSN Print: 2208-3502

Design and Simulation of a Microstrip Frequency-Scanning Antenna for Millimetre-Wave Fuze Applications

Qinyi Wang*

The University of New South Wales, Sydney 2052, Australia

**Author to whom correspondence should be addressed.*

Abstract: To satisfy the simultaneous requirements of high gain and wide angular coverage for millimetre-wave fuzes under large impact-angle variations, this paper proposes a microstrip frequency-scanning antenna based on a quasi-travelling-wave, series-fed patch array. The antenna is implemented on Rogers 4350B substrate ($\varepsilon r = 3.5$, thickness $h = 0.254$ mm) and operates over 30–36 GHz. By exploiting the frequency-dependent phase progression along the series feed, the main beam steers continuously without phase shifters. Full-wave simulations in HFSS show that the antenna maintains $|S11| < -10$ dB across the entire band. The E-plane main beam scans from 48° at 30 GHz to 0° at 36 GHz, providing a 48° frequency-scanning range; when the 3-dB beamwidth is included, the effective detection-angle coverage reaches approximately 74°. The simulated gain remains stable above 10.5 dBi, peaking at about 11.6 dBi near 35 GHz. With a low-profile, planar structure (overall size ≈ 20 mm × 10 mm) and no additional terminal load, the proposed design offers a compact solution for fuze antennas that require broad angular coverage and robust gain in the 30–36GHz.

Keywords: Millimetre-wave; Microstrip patch; Frequency-scanning antenna; Quasi-travelling wave; Series-fed microstrip array; HFSS

Online publication: February 12, 2026

1. Introduction

Millimetre-wave fuze sensing systems are attractive due to their compact size and high range resolution [1]. In practice, the fuze antenna must preserve effective target illumination and echo reception under significant variations in projectile attitude and impact angle [2]. This results in a challenging set of concurrent requirements: compact form factor, high gain, and wide angular coverage. Conventional waveguide slot arrays can provide high efficiency but are relatively bulky and heavy, where their scan capability is also limited, which complicates conformal integration on projectiles. In contrast, planar microstrip antennas are low-cost, lightweight, and suitable for conformal mounting, making them a promising candidate for fuze applications.

Existing fuze-antenna studies generally follow two routes. The first uses multi-beam or multi-port switching to obtain several discrete pointing directions [3]. The second relies on array phase control or frequency scanning to achieve continuous (or quasi-continuous) beam steering. While miniaturised multi-beam designs can realise multiple fixed tilt angles, they typically provide limited angular continuity and may introduce extra feed complexity. Frequency-scanning arrays, on the other hand, enable beam steering through intrinsic dispersion, thereby reducing system complexity. Motivated by Ka-band fuze scenarios (30–36 GHz), this work adopts a microstrip frequency-scanning array as a compact route to meet the practical objectives of constrained size, stable gain, and large detection-angle coverage.

The main contributions are as follows:

(1) A parameter-selection guideline is provided based on the phase condition of frequency-scanning arrays, covering patch dimensions, inter-element spacing, element count, and feedline width;

(2) With broadband impedance matching, the design achieves a 48° main-beam scan and ~74° effective coverage while maintaining a stable gain above 10.5 dBi.

In a typical millimetre-wave fuze, the antenna is installed on a compact projectile body and must operate reliably during high-speed flight and terminal engagement. The projectile attitude and the target aspect angle can change rapidly, so a fixed broadside beam may fail to maintain sufficient echo power at the receiver. From a system viewpoint, the antenna must deliver a stable gain within a wide angular sector, while remaining low-profile and mechanically robust.

Beam steering can be realised electronically (phase shifters, switched networks, or true-time-delay units), but these approaches increase cost, volume, and power consumption. Moreover, component tolerances and packaging parasitics become increasingly critical in the Ka-band. A frequency-scanning approach provides an alternative: the beam direction is controlled by frequency-dependent dispersion in the feed, eliminating phase-control circuits and improving system simplicity.

Related work on fuze antennas includes waveguide slot arrays, conformal patch arrays, multi-beam microstrip structures, and frequency-scanning arrays. Waveguide arrays generally offer high efficiency and high power handling, yet their height and mass can be difficult to accommodate on small platforms. Planar multi-beam designs (e.g., multi-port switching or pattern reconfiguration) provide several discrete pointing angles, but they do not naturally provide continuous coverage. Frequency-scanning arrays have been studied for radar and sensing, where an inherent frequency-angle mapping enables mechanical-free scanning. However, in fuze scenarios, the antenna must simultaneously satisfy compact size, acceptable matching over a wide band, and stable gain while scanning.

Compared with prior frequency-scanning implementations that rely on external loads or complex feeding networks, this manuscript emphasises a practical, fabrication-friendly design: a quasi-travelling-wave series-fed microstrip patch array with a load-free termination strategy. The design targets 30–36 GHz because this band offers a good balance between antenna size and atmospheric attenuation for short-range fuze sensing, and it aligns with commonly reported Ka-band fuze front-end architectures.

2. Frequency-scanning principle and design method

2.1. Principle of scanning mechanism

A frequency-scanning antenna is commonly realised using a uniform linear array [4]. The far-field main-beam direction is determined by the effective phase difference between adjacent radiating elements. As frequency

changes, the propagation constant and electrical length of the feed network change accordingly, which modifies the inter-element phase difference and therefore steers the main lobe [5]. For a series-fed microstrip patch array operating in a quasi-traveling-wave mode, adjacent elements are excited sequentially with a fixed physical separation d and an effective feeding-line length (d-L), where L denotes the patch length. The phase difference between two adjacent elements can be written as:

$$\varphi = \frac{2\pi}{\lambda_g}(d - L) \tag{1}$$

where λ_g is the guided wavelength along the microstrip line. In the far field, constructive interference in the direction theta requires the total phase difference between adjacent elements to satisfy the array phase condition

$$\begin{cases} -2\pi m = \frac{2\pi}{\lambda_1} d \sin\theta_1 - \frac{2\pi}{\lambda_{g1}}(d - L) \\ -2\pi m = \frac{2\pi}{\lambda_2} d \sin\theta_2 - \frac{2\pi}{\lambda_{g2}}(d - L) \end{cases} \tag{2}$$

where λ_0 is the free-space wavelength and m is the diffraction order.

Equation 2 establishes a direct relationship between the operating frequency, the inter-element spacing d, and the main-beam tilt angle theta. When (d-L) is fixed, variations in frequency modify both λ_0 and λ_g, resulting in a frequency-dependent beam direction. This mechanism forms the theoretical basis of frequency scanning.

To avoid the occurrence of grating lobes, the inter-element spacing must satisfy the well-known constraint, which limits the maximum allowable spacing for a given scanning angle.

$$d < \frac{\lambda_0}{1+|\cos\theta|} \tag{3}$$

Meanwhile, for a specified progressive phase difference \phi, the element spacing can also be expressed as:

$$d = -\frac{\varphi}{k\cos\theta} \tag{4}$$

where k is an integer related to the phase progression order.

Equation 3 and **Equation 4** jointly constrain the design space of the frequency-scanning array [3].

In the proposed antenna, a uniform linear array configuration is adopted, and all patch elements are excited using identical microstrip feeding lines. Owing to the traveling-wave nature of the structure, reflections along the feeding network are negligible. Therefore, the inter-element phase relationship can be effectively controlled by adjusting the physical length of the microstrip line, which directly determines the phase difference.

By properly selecting the inter-element spacing d, the main-beam direction can be steered toward either the feeding end or the load end [5]. Specifically, when d < λ_g, the main beam tends to tilt toward the feeding end, whereas for d >λ_g it tilts toward the load end. In practical implementations, a relatively small spacing d is preferred to achieve beam steering toward the feeding end while simultaneously enabling antenna miniaturization.

2.2. Key parameter selection

The parameters are as follows:

(1) Patch dimensions: A cavity-model approximation with an effective permittivity εeff is used to initialise the rectangular patch size so that the centre frequency is around 33 GHz;

(2) Inter-element spacing d: Increasing d generally enlarges the scan range by strengthening the phase

gradient, but it may degrade matching and increase the risk of grating lobes; thus d is chosen by balancing scan range, matching, and pattern integrity;

(3) Element number N: Larger N increases gain and narrows the beam, but also increases series-feed loss and overall length. To satisfy gain ≥ 10 dB under size constraints, this work selects N = 6.

Patch initialisation uses standard transmission-line/cavity-model relations. Given a target centre frequency f_0 and substrate relative permittivity εr, the patch width is approximated by:

$$W = \frac{c}{2f_0}\left(\frac{\varepsilon_r + 1}{2}\right)^{-\frac{1}{2}}$$

The effective permittivity εeff is then estimated to account for fringing fields, and the effective length Leff is approximated as:

$$L = \frac{c}{2f_0\sqrt{\varepsilon_e}} - 2\Delta l:$$

The physical length L is obtained by subtracting the fringing extension (2ΔL). These closed-form steps provide a reliable starting point for full-wave optimization [6].

Substrate selection is critical in the Ka-band. A lower-loss laminate reduces dielectric loss and improves radiation efficiency, while a thinner substrate suppresses surface waves and helps maintain pattern stability. Rogers 4350B is selected because it offers a moderate permittivity (εr ≈ 3.5) that keeps the antenna compact without making the feed excessively narrow, and it provides a low loss tangent suitable for millimetre-wave prototypes. The thickness h = 0.254 mm further reduces profile and mitigates surface-wave excitation.

Inter-element spacing d is chosen below one free-space wavelength to avoid grating lobes over the scan range [7]. Using λ_0 ≈ 10 mm at 30 GHz, the selected d = 3.4 mm corresponds to about 0.34 λ0, which provides a good trade-off between mutual coupling control and sufficient phase gradient for scanning. The element number N is set to 6 to obtain a stable gain above 10 dBi while limiting series-feed loss and overall size [8].

3. Antenna configuration and parameters

3.1. Structure

The proposed antenna is a single-layer, series-fed microstrip patch array. Rectangular patches are cascaded along the array axis and excited by a microstrip feedline at the input port. Instead of attaching an explicit terminal load, the end section is shaped to provide an equivalent dissipative behaviour through distributed loss, which helps suppress reflections and improves matching. The substrate is Rogers 4350B (εr = 3.5, h = 0.254 mm). The overall footprint is approximately 20 mm × 10 mm, which is suitable for compact projectile integration.

The series-fed architecture is implemented using microstrip line segments that excite each patch sequentially. To maintain consistent phase progression and reduce discontinuity reflections, the feedline widths are chosen according to the required characteristic impedance and manufacturability. A wider input line (y1) helps reduce conductor loss near the feed, while a narrower inter-element line (y2) enables finer impedance transformation and phase control between adjacent patches.

A practical termination is designed at the end of the feed to suppress reflections. Rather than adding an external chip load (which can be challenging to source and mount reliably at 30–36 GHz, the terminal section is shaped so that residual power is dissipated through distributed conductor/dielectric losses and weak radiation. This

approach improves robustness and repeatability for compact antenna modules.

From a fabrication perspective, the minimum line width and gap are kept compatible with standard PCB processes for Rogers laminates. Because the substrate is thin, the design is sensitive to etching tolerance and copper roughness. The layout therefore avoids extremely narrow traces and abrupt right-angle corners. In future hardware validation, a calibration kit and a low-loss end-launch connector (or a probe-fed fixture) would be required to measure |S11| accurately in the Ka-band.

3.2. Optimisation workflow

The optimisation follows a practical order: "element first, array next; resonance first, scan next". The patch width W and length L are tuned to place the resonance within the target band. Followed by that is the input feedline width y1 and inter-element feedline width y2 are adjusted to obtain broadband impedance matching. Finally, under the constraint $|S11| < -10$ dB across 30–36 GHz, the spacing d is refined to trade off gain, scan range, and pattern stability. This staged workflow reduces multi-parameter coupling and improves engineering reusability.

4. Simulation setup and results

4.1. Simulation model

Based on the theoretical calculation parameters listed in **Table 1** and the antenna structural, the antenna model is established using the ANSYS HFSS electromagnetic simulation software, as illustrated in **Figure 1**. The overall substrate size of the antenna is 20 mm × 10 mm. During the modeling process, boundary conditions and excitation are defined sequentially. The microstrip patch elements and the bottom ground plane are set as ideal conducting boundaries (Perfect E). The excitation is implemented in the form of a lumped port with concentrated terminal feeding (Lumped Port). According to the antenna dimensions, a suitable air box is constructed around the antenna and assigned a radiation boundary condition (Radiation).

Table 1. Optimised key parameters (unit: mm)

W	L	d	y1	y2	Substrate h	N
3.8	2.2	3.4	0.50	0.35	0.254	6

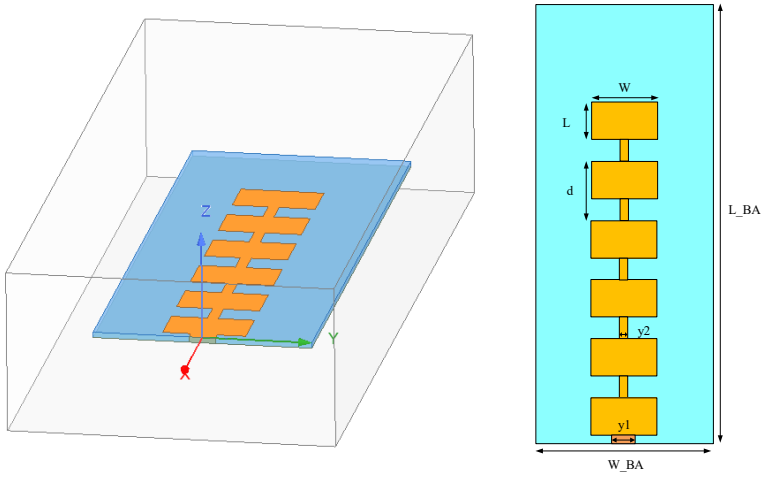

Figure 1. Structural model of the microstrip frequency-scanning antenna.

To excite the microstrip patch elements, a microstrip line is used for direct feeding, and a single-ended feeding configuration is adopted. By adjusting the width y_1 and length d_1 of the input microstrip line, as well as the width y_2 of the inter-element microstrip line between adjacent patch elements, impedance matching of the antenna to 50 Ω can be achieved. After initial simulation optimization, the input microstrip line width y_1 is set to 1.0 mm, the input line length d_1 is set to 0.5 mm, and the inter-element microstrip line width y_2 is set to 0.5 mm.

4.2. Parameter optimization

4.2.1. Frequency optimization

According to the calculation formula derived, it can be concluded that the resonant frequency of the antenna is mainly influenced by the length W and width L of the rectangular patch element. As the operating frequency increases, the dimensions of the patch element decrease, i.e., both W and L become smaller. Conversely, as the operating frequency decreases, the patch dimensions increase, corresponding to larger values of W and L.

4.2.2. Impedance-matching optimization

The matching objective is a 50-Ω input with |S_{11}|<-10 dB across 30–36 GHz. Since the initial design does not satisfy this requirement at several frequencies, the matching network is refined by tuning the input feed-line width y_1, the feed-line length d_1, and the inter-element microstrip width y_2. These parameters are co-optimized to stabilize the impedance response over the entire band.

4.2.3. Gain optimization

The realized gain is mainly determined by the inter-element spacing d and the element number N. The spacing d is optimized to achieve a favorable trade-off between gain level and frequency-scanning behavior (beam angle versus frequency), while maintaining acceptable matching.

4.2.4. Element-number selection

A small N provides wider scanning bandwidth but yields insufficient low-frequency gain (< 10 dB). Increasing N improves gain [9]. However, overly large N exacerbates return loss and disrupts impedance matching, which in turn degrades the frequency-scanning characteristic and reduces effective scanning bandwidth and main-beam coverage. Considering these trade-offs, N = 6 is selected as the optimal configuration.

4.3. Simulation results and analysis

Based on the optimization procedure described above, a quasi–traveling-wave millimeter-wave microstrip frequency-scanning antenna with an inter-element spacing of d = 3.4mm and an element number of N = 6 is finalized. The antenna exhibits a frequency-dependent main-beam steering behavior, in which the main-beam tilt angle θ varies monotonically with operating frequency. As a result, the E-plane effective main-beam coverage exceeds 70°, ensuring robust target detection capability for fuze applications under a wide range of impact-angle conditions.

To verify compliance with the design specifications, the simulated results are analyzed in terms of the reflection coefficient, E-plane radiation patterns, and the frequency-dependent scanning radiation characteristics of the antenna.

4.3.1. S parameter

Figure 2 shows the simulated reflection coefficient of the six-element frequency-scanning antenna. It is observed that S11 remains below −10 dB throughout the operating band from 30 to 36 GHz, indicating good impedance matching across the entire frequency range. This confirms that the optimized feeding network successfully achieves a stable 50Ω input impedance over the desired bandwidth.

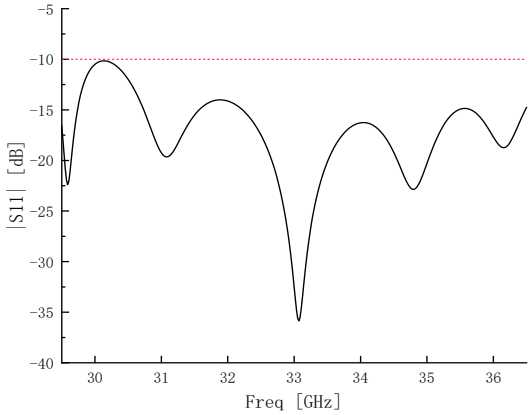

Figure 2. S11 curve.

4.3.2. E-plane radiation patterns

To evaluate the radiation performance, E-plane radiation patterns are extracted at six representative frequencies within the operating band, namely 31, 32, 33, 34, 35, and 36 GHz, with \phi = 0^\circ and \theta ranging from −180° to 180°, as shown in **Figure 3**.

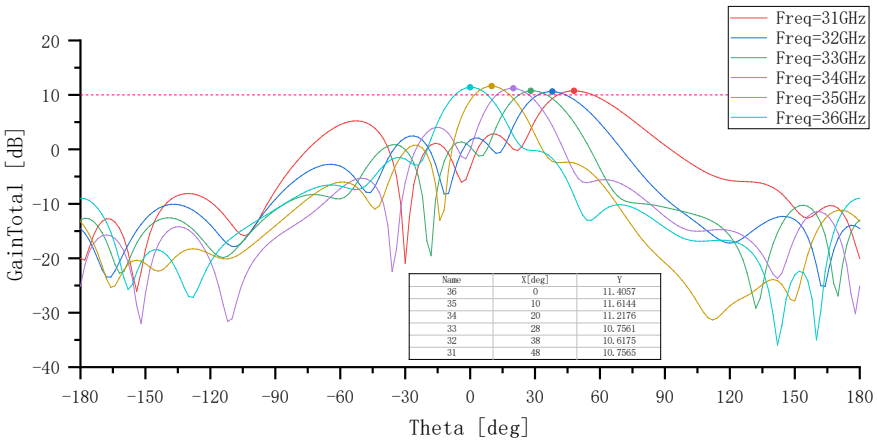

Figure 3. E-plane radiation patterns.

The results demonstrate that the antenna gain at all selected frequencies exceeds 10 dB, satisfying the design requirement. As the operating frequency increases from 30 to 36 GHz, the main-beam tilt angle continuously shifts from approximately 48° toward broadside (0°), confirming the intended frequency-scanning behavior. The maximum realized gain of approximately 11.6 dB is achieved at 35 GHz.

4.3.3. Frequency-scanning performance

Figure 4 presents the E-plane radiation pattern at the center frequency of 33 GHz.

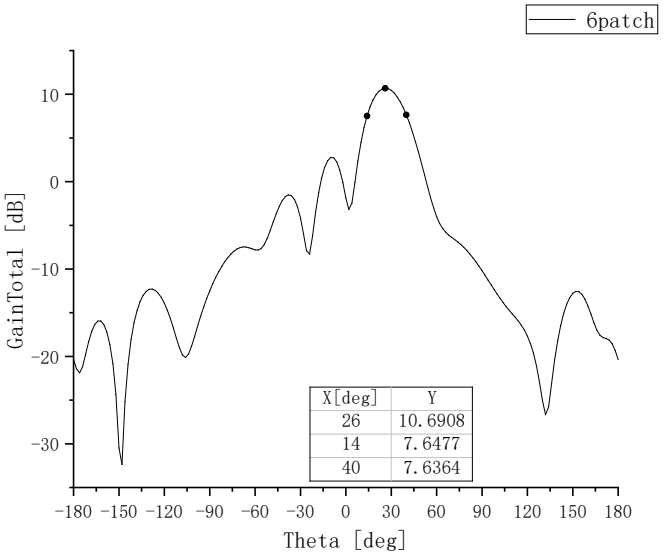

Figure 4. E-plane radiation pattern at 33 GHz.

At this frequency, the main-beam tilt angle is approximately 26°, and the E-plane half-power beamwidth (HPBW) is about 26°. Over the operating band from 30 to 36 GHz, the main-beam direction scans from 48° to 0°, corresponding to a scanning range of 48°. Considering the HPBW of approximately 26°, the effective E-plane main-beam coverage angle reaches about 74°, providing wide angular coverage suitable for millimeter-wave fuze applications.

5. Conclusion

From an engineering perspective, the design demonstrates a low-complexity route to obtain broad angular coverage in the Ka-band without resorting to bulky waveguides or active phase-control circuits, which can be advantageous for compact and high-reliability fuze sensing modules. A compact Ka-band microstrip frequency-scanning antenna for fuze applications has been presented. Based on a quasi-travelling-wave series-fed patch array on Rogers 4350B, the design achieves broadband matching ($|S11| < -10$ dB over 30–36 GHz), stable gain above 10.5 dBi (peak ≈ 11.6 dBi), and continuous E-plane beam steering from 48° to 0°. By incorporating the 3-dB beamwidth, the effective detection-angle coverage reaches ~74°, which is beneficial under large impact-angle variations. Future work will include conformal installation analysis on projectile bodies, sidelobe suppression via spacing tapering or amplitude weighting, and fabrication/measurement validation with tolerance-aware modelling. As the beam direction is frequency dependent, a practical fuze radar can exploit frequency selection to choose the desired pointing direction on demand. For example, lower frequencies in the 30–36 GHz band correspond to larger tilt angles, while higher frequencies steer the beam closer to broadside in this design. This enables a simple scan strategy where the transmitter steps through several frequency points to cover the sector, and the receiver combines echoes accordingly. Such an approach is compatible with agile frequency synthesizers and can be implemented without adding RF phase-control hardware.

Disclosure statement

The author declares no conflict of interest.

References

[1] Liu Y, 2009, Research and Design of Microstrip Frequency-Scanning Antenna Arrays, thesis, Nanjing Univ. Sci. Technol.

[2] Wang Q, 2019, Design of Miniaturized Radio Fuze Antennas, thesis, Nanjing Univ. Sci. Technol.

[3] Fu Y, 2015, Research on Millimeter-Wave Frequency-Scanning Antennas, thesis, Harbin Inst. Technol.

[4] Wang D, Wang Z, Xu L, et al., 2017, A Millimeter-Wave Microstrip Frequency-Scanning Fuze Antenna Based on a Quasi-Traveling-Wave Array. Bingqi Zhuangbei Gongcheng Xuebao (Journal of Ordnance Equipment Engineering), 38(6): 156–160.

[5] Liu J, Wu D, Yao M, 2008, Design of Millimeter-Wave Waveguide Slot Antennas. Journal of Ordnance Engineering, 29(2): 15–17.

[6] Wang Y, Zhang L, Kou D, 2004, Design of Wideband Waveguide Slot Antennas. Journal of Ordnance Engineering, 25(2): 37–41.

[7] Li Z, 2021, Design of Wireless Radio-Frequency Waveguide Antennas, thesis, Nanjing University of Science and Technology.

[8] He L, 2016, Thermal Design of Airborne Millimeter-Wave Active Phased Array Antennas. Journal of Ordnance Equipment Engineering, 37(5): 115–119.

[9] Zhou X, 2006, Simulation Design and Error Analysis of Millimeter-Wave Fuze Antennas. Zhi Dao Yu Yin Xin (Guidance and Fuze), 27(4): 28–31.